Direct energy cascade in two-dimensional compressible quantum turbulence

Ryu Numasato and Makoto Tsubota
Department of Physics, Osaka City University, Sumiyoshi-ku, Osaka 558-8585, Japan

Victor S. L'vov
Department of Chemical Physics, The Weizmann Institute of Science, Rehovot 76100, Israel

(Received 18 February 2010; published 24 June 2010)

We numerically study two-dimensional quantum turbulence with a Gross-Pitaevskii model. With the energy initially accumulated at large scale, quantum turbulence with many quantized vortex points is generated. Due to the lack of enstrophy conservation in this model, direct energy cascade with a Kolmogorov-Obukhov energy spectrum $E(k) \propto k^{-5/3}$ is observed, which is quite different from two-dimensional incompressible classical turbulence in the decaying case. A positive value for the energy flux guarantees a *direct* energy cascade in the inertial range (from large to small scales). After almost all the energy at the large scale cascades to the small scale, the compressible kinetic energy realizes the thermodynamic equilibrium state without quantized vortices.

DOI: 10.1103/PhysRevA.81.063630 PACS number(s): 03.75.Hh, 67.25.dk, 47.37.+q

I. INTRODUCTION

The experimental discovery of Bose-Einstein condensates (BECs) 15 years ago [1–3], long after their theoretical prediction in the 1920s, has renewed interest in this field. BEC systems are of great interest as they promise the opportunity to study new nonlinear dynamical systems built with a high degree of control and flexibility. Also, theoretical and numerical studies of BEC systems are of general importance for nonlinear physics, as BEC systems are described by one of the most important and universal partial differential equations, the nonlinear Schrödinger equation, called in this field the Gross-Pitaevskii (GP) equation (GPE) [4,5]:

$$i\frac{\partial \Psi}{\partial t} + \frac{1}{2}\nabla^2\Psi - \frac{1}{2}g|\Psi|^2\Psi = 0. \quad (1)$$

Here the condensate wave function $\Psi(\boldsymbol{r},t)$ plays the role of the complex order parameter. The parameter g is the strength of contact interaction of the two particles, being $4\pi\hbar^2 a/m$ in the dimensional GPE, where a is the s-wave scattering length and m is the mass of the atom.

This work is based on two-dimensional (2D) dynamics. We numerically solve 2D GPE, and we assume a 2D BEC which is dynamically frozen in the transversal direction. In experiments, a pancake-shaped BEC, which is strongly trapped along the z axis, satisfies this situation. Section II describes the detail of the validity of 2D GP model.

The GPE (1) describes a Bose gas at low temperature, which may behave similarly to a superfluid, and can describe its random (turbulent) motion, that is, quantum turbulence (QT). QT physics, comprising tangled quantized vortices, is an important research topic in low-temperature physics [6,7]. Stimulated by recent experiments on both superfluid ^{3}He and superfluid ^{4}He, where a few similarities have been observed between quantum and classical turbulence [8–15], studies on QT have entered a new stage where one of the main motivations is to investigate the relationship between quantum and classical turbulence. In particular, the Kolmogorov-Obukhov turbulent kinetic energy spectrum $E(k) \propto k^{-5/3}$ has been observed in laboratory experiments on superfluid ^{4}He similar to that in normal fluids [16]. The physical explanation for this is very simple: For superfluid motion at scales $\mathcal{L}$ essentially exceeding the mean intervortex distance ℓ, the quantization of the vortex lines can be neglected. This range of scales corresponds to the quasiclassical limit and this type of turbulence can be called *quasiclassical turbulence* (QCT). QCT in the three-dimensional (3D) case has subsequently been found in numerical simulations with the GPE as well as in the vortex filament model [17] that can describe motions of quantized vortex lines with a prescribed core structure.

It is well known that Euler equations, which describe motion of ideal (inviscid) fluids, in the 2D case exhibit an additional second quadratic motion invariant, enstrophy Ω, as well as kinetic energy E:

$$E \equiv \frac{1}{2}\int |\boldsymbol{v}|^2 d\boldsymbol{r}, \quad \Omega \equiv \int \omega^2 d\boldsymbol{r}, \quad \omega \equiv [\nabla \times \boldsymbol{v}]_z. \quad (2)$$

Kraichnan recognized [18] that the appearance of Ω drastically modifies the physics of 2D turbulence. It changes the direction of the energy flux in the classical Richardson-Kolmogorov cascade. Instead of a *direct* energy cascade (from large to small scales), like in 3D turbulence, in the 2D case there is an *inverse* energy cascade, from small to large scales. In both the 3D and 2D cases the energy spectrum is the same, $E(k) \propto k^{-5/3}$. In 2D turbulence the direct *energy* cascade is replaced by the direct enstrophy cascade with the energy spectrum $E(k) \propto k^{-3}$ (subject to certain logarithmic corrections, unimportant in the current discussion). These predictions have been confirmed in laboratory experiments (see, e.g., Ref. [19]) and using large-scale direct numerical simulations (DNS) of the Navier-Stokes equations (see, e.g., Refs [20–22]).

An important issue is whether the inverse energy cascade is a feature of 2D QT. The qualitative answer given in our paper is "not necessarily." The physical reason for this is quite simple and general.

In superfluids, the enstrophy Ω coincides (up to a prefactor) with the total number of quantized vortex points [23]. In GP dynamics the total number of vortices is not conserved. They can appear in pair creation or disappear in pair annihilation. Therefore, Kraichnan's arguments [18] become, generally

speaking, irrelevant for 2D QT. Thus, for a certain range of parameters, where the creation or annihilation of vortex pairs become dynamically important, we can expect a *direct* energy cascade in 2D QT, exactly as in 3D classical turbulence. This is an important conclusion of our paper. Simulating the free evolution of 2D GPE (from an initial condition with energy located at large scales) we observed a *direct* energy cascade with the Kolmogorov-Obukhov energy spectrum $E(k) \propto k^{-5/3}$.

The same argument can be made based on Euler equations. Indeed, the superfluid density in the vicinity of a vortex core is different from that in a vortex-free superfluid. Therefore the creation or annihilation of vortex pairs lead to variations of the superfluid density. In other words, the GPE is reduced to a compressible Euler equation. However, a compressible Euler equation does not preserve enstrophy. Therefore at some level of compressibility (characterized by the Mach number, the ratio of the turbulent velocity fluctuations to the sound velocity) the direction of the energy flux can change sign and, instead of an inverse energy cascade, we observe a direct cascade, typical for 3D turbulence.

In this study, we observe the direct energy cascade in numerical experiments with 2D GPE. Starting from initial conditions with energy localized at large scales we observed an intermediate asymptotic Richardson cascade transporting energy of the system toward small scales. The energy spectrum at this stage is close to the Kolmogorov-Obukhov law $E(k) \propto k^{-5/3}$. At later stages, when an essential part of the energy reaches the smallest scales available in our simulations (mean intervortex spacing, which is a few times larger than the core diameter), the system quickly evolves toward thermodynamic equilibrium. As an independent test of the direction of the energy flux we analyzed the energy balance equation in k space and found that the sign of the energy flux indeed corresponds to the direct cascade.

In addition, we studied the properties of the finite steady state of the system by a different means (e.g., by analyzing the power spectra in the frequency domain for motion with different wave vectors). We show that the position of the maximum of the power spectra $\omega_{\max}(k)$ depends on the dispersion relation derived from Bogoliubov's microscopic theory [4,5].

In addition, we investigate how the time evolution of the system depends on the level of nonlinearity by qualitatively comparing its behavior with the same initial conditions but different coupling constants g.

The paper is organized as follows. After this introduction, in Sec. II we discuss the validity of the 2D GP model. In Sec. III we explain the analytical and numerical formulations of the GP model of compressible quantum turbulence. Next, in Sec. IV we explain the turbulent state (i.e., the time development of the energy, kinetic energy spectra, and incompressible kinetic energy flux). We also show how the direct energy cascade with the Kolmogorov-Obukhov law is formed and prove the direct energy cascade with the use of the approximated incompressible kinetic energy flux. Then, through numerical analysis of the power spectrum of the compressible effective velocity, we find that Bogoliubov's microscopic theory holds in the thermodynamic equilibrium state full of compressible kinetic energy. Finally, in Sec. V we state the conclusions of the paper.

II. THE VALIDITY OF THE 2D GP MODEL

In this paper, we use 2D GPE in a uniform system. However, in experiments, the BEC is always trapped, typically in a harmonic potential. This situation is realized in a pancake-shaped potential. The 3D GPE with this potential is reduced to the wave function in x-y space and on the z axis [24]. The strength of the trap along the z axis is determined by the ratio $\lambda \equiv \omega_z/\omega_\perp$. Here ω_z and $\omega_\perp$ are the oscillator frequencies on the z axis and in x-y space, respectively, and a pancake-shaped potential means $\lambda \gg 1$. If $\hbar\omega_z$ is larger than the chemical potential, the wave function along the z axis can be approximated by a Gaussian function. Through the reduction of 3D GPE into the x-y space and the z axis, we obtain the nondimensional strength of interaction C, which is expressed as g in this paper,

$$C = 4\sqrt{\pi\lambda}N\frac{a}{a_h}. \tag{3}$$

Here N is the total particle number and a_h is the horizontal width of the BEC, $\sqrt{\hbar/2m\omega_\perp}$.

With Eq. (3), we estimate the value of C for realistic cases. If we take $m = 1.46 \times 10^{-25}$ kg, $a = 5.77$ nm, $N = 10^3$, $\omega_z = 100$ Hz, $\lambda = 10$, and $a_h = 6.01$ μm, then C becomes ~ 20. In order to take the characteristic phenomena, we will make the numerical simulation chiefly with $g = 1$, 2, and 4, although these values are smaller than the estimated value of C. In [24], the nondimensional time $\tilde{t}$ is $t\omega_\perp$. As shown in Fig. 4 later, the characteristic time scale is close to the BEC lifetime, thus the phenomena reported in this paper could be observed in realistic experiments.

III. THE GP MODEL OF COMPRESSIBLE TURBULENCE

A. GP and "quantum" Euler equations

It is well known [4,5] that GPE conserves the total energy (Hamiltonian) H and "particle number" N:

$$H = \int \left[\frac{1}{2}|\nabla\Psi|^2 + \frac{1}{4}g|\Psi|^4\right] d\boldsymbol{r}, \tag{4a}$$

$$N = \int |\Psi|^2 d\boldsymbol{r}. \tag{4b}$$

By analogy with the Schrödinger equation we can consider the probability $|\Psi(\boldsymbol{r},t)|^2$ as a particle density:

$$\rho(\boldsymbol{r},t) \equiv |\Psi(\boldsymbol{r},t)|^2. \tag{5a}$$

Then the conservation law of N can be considered as the conservation of the total mass of the system, $M \equiv \int \rho d\boldsymbol{r} = N$ (under the assumption that the "particle mass" is unity), which can be written as a continuity equation:

$$\frac{\partial\rho}{\partial t} + \nabla\cdot\boldsymbol{j} = 0. \tag{5b}$$

Here $\boldsymbol{j}$ is the particle flux,

$$\boldsymbol{j} \equiv \frac{i}{2}(\Psi\nabla\Psi^* - \Psi^*\nabla\Psi), \tag{5c}$$

which can be presented in the familiar form $\boldsymbol{j} = \rho\boldsymbol{v}$ with the "fluid" velocity:

$$\boldsymbol{v} = \nabla\theta. \tag{5d}$$

Here the phase θ is defined via the Madelung transformation:

$$\Psi = \sqrt{\rho}\exp(i\theta), \tag{5e}$$

which maps the GPE (1) to the Euler equation for an ideal compressible fluid with an extra quantum pressure term.

B. Decomposition of the system energy

Following Ref. [14] it is instructive to decompose the total energy of the system H, Eq. (4a), conserved by GPE (1), into four parts. The first part originates from the interaction energy in the Hamiltonian (4a) of the GPE (1) with the density $g|\Psi|^4/4 = g\rho^2/4$. Bearing in mind that $\int \rho d\boldsymbol{r} = \text{const.}$, we can introduce the density of the "internal energy" as $g\rho^2/4$ counted from $(g/2)(\rho - \frac{1}{2})$:

$$\mathcal{E}_{\text{int}}(\boldsymbol{r}) \equiv \frac{g}{4}(\rho - 1)^2. \tag{6}$$

Next, we define the density of the fluid kinetic energy as usual:

$$\mathcal{E}_{\text{kin}}(\boldsymbol{r}) \equiv \tfrac{1}{2}\rho|\boldsymbol{v}|^2 \equiv \tfrac{1}{2}|\boldsymbol{w}|^2, \quad \boldsymbol{w} \equiv \sqrt{\rho}\boldsymbol{v}. \tag{7a}$$

This kinetic energy can be divided into compressible and incompressible parts by decomposing the effective "velocity" field $\boldsymbol{w}$ into divergent free $\boldsymbol{w}^{\text{i}}$ and potential $\boldsymbol{w}^{\text{c}}$ parts:

$$\mathcal{E}_{\text{kin}}(\boldsymbol{r}) = \mathcal{E}^{\text{i}}_{\text{kin}}(\boldsymbol{r}) + \mathcal{E}^{\text{c}}_{\text{kin}}(\boldsymbol{r}), \tag{7b}$$

$$\mathcal{E}^{\text{i}}_{\text{kin}}(\boldsymbol{r}) \equiv \tfrac{1}{2}|\boldsymbol{w}^{\text{i}}|^2, \quad \mathcal{E}^{\text{c}}_{\text{kin}}(\boldsymbol{r}) \equiv \tfrac{1}{2}|\boldsymbol{w}^{\text{c}}|^2, \tag{7c}$$

because $\boldsymbol{w}^{\text{i}} \cdot \boldsymbol{w}^{\text{c}} \equiv 0$.

Now, the first term in the Hamiltonian (4a) in the representation of (5d), (5e) can be presented as follows:

$$\begin{gathered}\tfrac{1}{2}|\nabla\Psi|^2 = \tfrac{1}{2}[\rho|\boldsymbol{v}|^2 + |\nabla\sqrt{\rho}|^2] = \mathcal{E}_{\text{kin}}(\boldsymbol{r}) + \mathcal{E}_{\text{qnt}}(\boldsymbol{r}) \\ \mathcal{E}_{\text{qnt}}(\boldsymbol{r}) \equiv \tfrac{1}{2}|\nabla\sqrt{\rho}|^2.\end{gathered} \tag{8}$$

The second term here, $\mathcal{E}_{\text{qnt}}(\boldsymbol{r})$, has been termed the *quantum* energy density [15].

Finally, the total (conserved) energy of the system can be decomposed into four parts:

$$H = \int \left[\mathcal{E}_{\text{int}}(\boldsymbol{r}) + \mathcal{E}^{\text{i}}_{\text{kin}}(\boldsymbol{r}) + \mathcal{E}^{\text{c}}_{\text{kin}}(\boldsymbol{r}) + \mathcal{E}_{\text{qnt}}(\boldsymbol{r})\right] d\boldsymbol{r}. \tag{9}$$

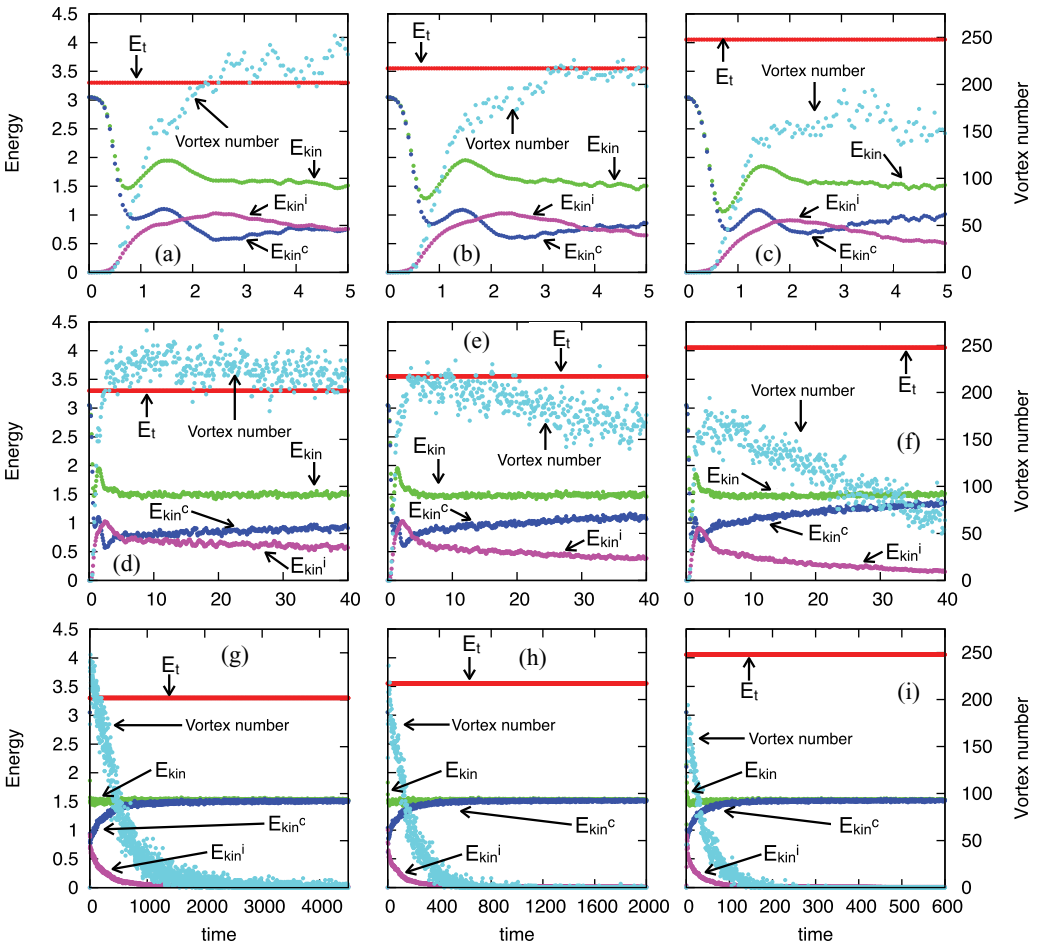

FIG. 1. (Color online) Time evolution of the dimensionless total energy E_{t}, total kinetic energy E_{kin}, and its compressible $E^{\text{c}}_{\text{kin}}$ and incompressible $E^{\text{i}}_{\text{kin}}$ parts. All energies are normalized with the particle number N, as shown in Eqs. (11). The time dependence of the total vortex number (a measure of the enstrophy) is also shown. Left panels: $g = 1$. Middle panels: $g = 2$. Right panels: $g = 4$. Upper panels: Initial evolution, $t \leqslant 5$. Middle panels: Intermediate stage, $t \leqslant 40$. Lower panels: Latest stage, $t \leqslant 4500$ for $g = 1$, $t \leqslant 2000$ for $g = 2$, and $t \leqslant 600$ for $g = 4$.

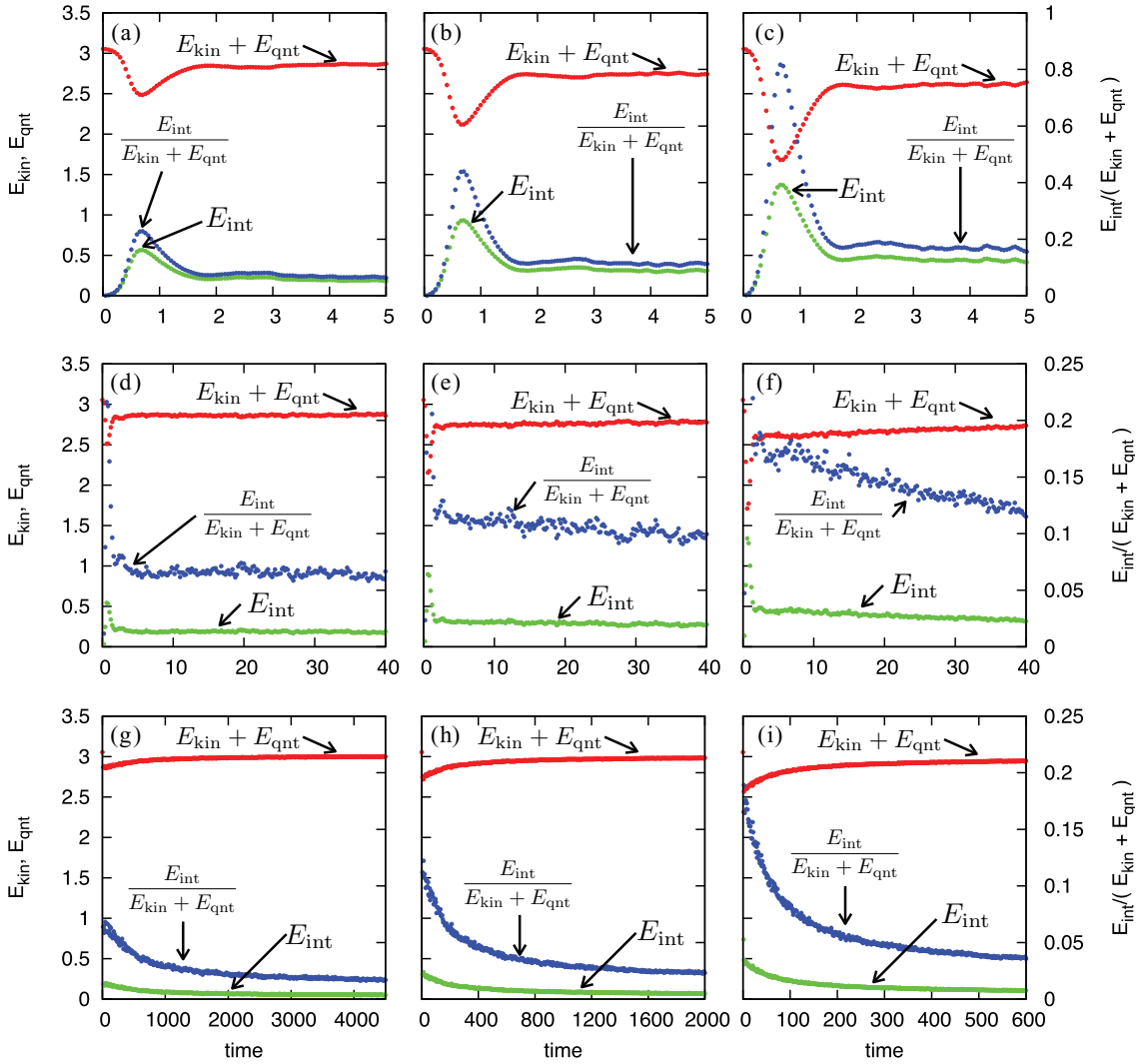

FIG. 2. (Color online) Time evolution of the interaction energy $E_{\rm int}$ [Eq. (6)], the sum of the total kinetic energy and quantum energies [Eqs. (7) and (8)], and the dimensionless nonlinearity level, R [Eq. (17)]. All energies are normalized with the particle number N, as shown in Eqs. (11). Left panels: $g = 1$/Middle panels: $g = 2$. Right panels: $g = 4$. Upper panels: Initial evolution, $t \leqslant 5$. Middle panels: Intermediate stage, $t \leqslant 40$. Lower panels: Latest stage, $t \leqslant 4500$ for $g = 1$, $t \leqslant 2000$ for $g = 2$, and $t \leqslant 600$ for $g = 4$.

C. Numerical procedure

We solve the 2D GPE (1) by the pseudo-spectral method in the domain 256^2 with the fourth-order Runge-Kutta method for the time development. For details, see Ref. [9].

To generate large-scale turbulent flow, the initial condition of the wave function is set to the random phase state $\Psi(\boldsymbol{r},0) = \exp[i\theta(\boldsymbol{r},0)]$ with

$$\tilde{\theta}(\boldsymbol{k},0) = \begin{cases} \theta_0 \exp[i\alpha(\boldsymbol{k})] & (\Delta k \leqslant |\boldsymbol{k}| \leqslant 3\Delta k), \\ 0 & (\text{otherwise}). \end{cases} \tag{10}$$

Here $\tilde{\theta}(\boldsymbol{k},0) = \tilde{\theta}^*(-\boldsymbol{k},0)$, $\alpha(\boldsymbol{k})$ is randomly taken for each $\boldsymbol{k}$ in the range $(-\pi,\pi)$, and $\Delta k = 2\pi/L$ is the wave number grid. The initial density is uniform, $|\Psi(\boldsymbol{r},0)|^2 = 1$. The phase distribution (10) is energetically high and unstable so that many quantized vortex pairs are created. With these initial conditions we obtain, during time evolution, a 2D QT composed of a random configuration of quantized vortices.

To investigate the character of the 2D QT we evolve the GPE (1) as described here and compute the following:

1. Time evolution of all four total energy components (9) per total particle number N and total vortex number $\mathcal{N}_{\rm qv}$ for different values of the coupling constant $g = 1, 2, 4$, shown in Fig. 1.

2. Time evolution of the dimensionless "level of nonlinearity," defined as $E_{\rm int}/(E_{\rm kin}+E_{\rm qnt})$, shown in Fig. 2.

3. Compressible and incompressible kinetic energy spectra, $E^{\rm c}_{\rm kin}(k)$ and $E^{\rm i}_{\rm kin}(k)$, shown for $g = 1, 2, 4$ in Figs. 3 and 4 and defined as

$$E^{\rm c}_{\rm kin}(t) = \frac{1}{2N}\int |\tilde{\boldsymbol{w}}^{\rm c}(\boldsymbol{k})|^2 d\boldsymbol{k} \equiv \int E^{\rm c}_{\rm kin}(k)\,dk, \tag{11a}$$

$$E^{\rm i}_{\rm kin}(t) = \frac{1}{2N}\int |\tilde{\boldsymbol{w}}^{\rm i}(\boldsymbol{k})|^2 d\boldsymbol{k} \equiv \int E^{\rm i}_{\rm kin}(k)\,dk, \tag{11b}$$

$$1 = \frac{1}{N}\int |\tilde{\Psi}(\boldsymbol{k})|^2 d\boldsymbol{k} \equiv \int N(k)\,dk, \tag{11c}$$

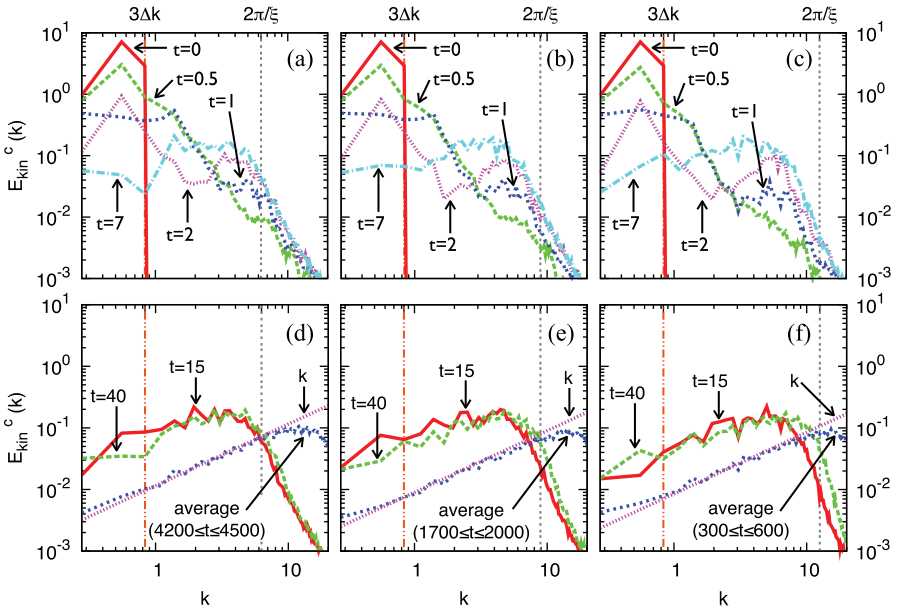

FIG. 3. (Color online) Log-log plots of the spectra of compressible kinetic energy at earlier (upper panels) and later (lower panels) moments of time. Left panels: $g = 1$. Middle panels: $g = 2$. Right panels: $g = 4$.

where

$$\tilde{w}^{\mathrm{c}}_{\alpha}(\boldsymbol{k}) = \sum_{\beta=1,2} \frac{k_\alpha k_\beta}{k^2} \tilde{w}_\beta(\boldsymbol{k}), \tag{11d}$$

$$\tilde{w}^{\mathrm{i}}_{\alpha}(\boldsymbol{k}) = \sum_{\beta=1,2} \left(\delta_{\alpha\beta} - \frac{k_\alpha k_\beta}{k^2}\right) \tilde{w}_\beta(\boldsymbol{k}). \tag{11e}$$

4. The spectra $E^{\mathrm{c}}_{\mathrm{kin}}(k)$, $E^{\mathrm{i}}_{\mathrm{kin}}(k)$, and $N(k)$ for different moments of time and different values of g, shown in Figs. 3, 4, and 5, respectively.

5. Mean incompressible kinetic energy flux in k space, $\varepsilon^{\mathrm{i}}(k)$, shown in Fig. 6 ($g = 1, 2, 4$).

6. Distribution of vortex-pair separations, shown for $g = 1, 2, 4$ in Fig. 7.

7. Frequency spectra of compressible and incompressible velocity components for different k and different g at later time moments, shown in Figs. 8 and 10, respectively, with positions of the maxima of the compressible frequency spectra $\omega_{\max}(k)$ shown in Fig. 9 for different g and different moments of time.

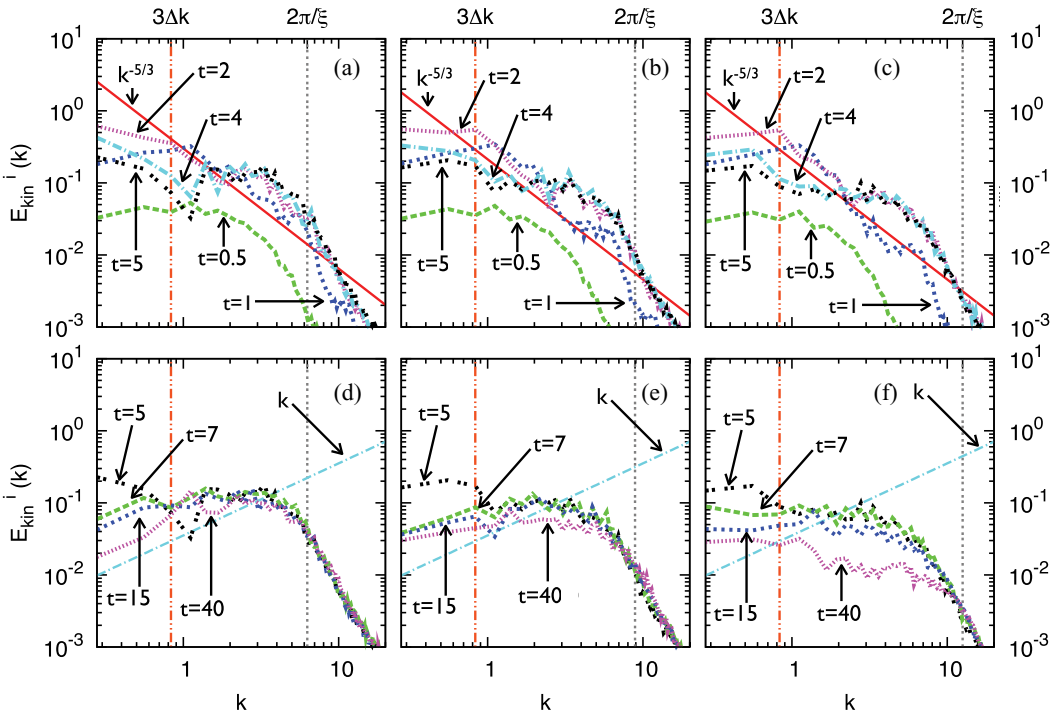

FIG. 4. (Color online) Log-log plots of the spectra of incompressible kinetic energy at earlier (upper panels) and later (lower panels) moments of time. Left panels: $g = 1$. Middle panels: $g = 2$. Right panels: $g = 4$.

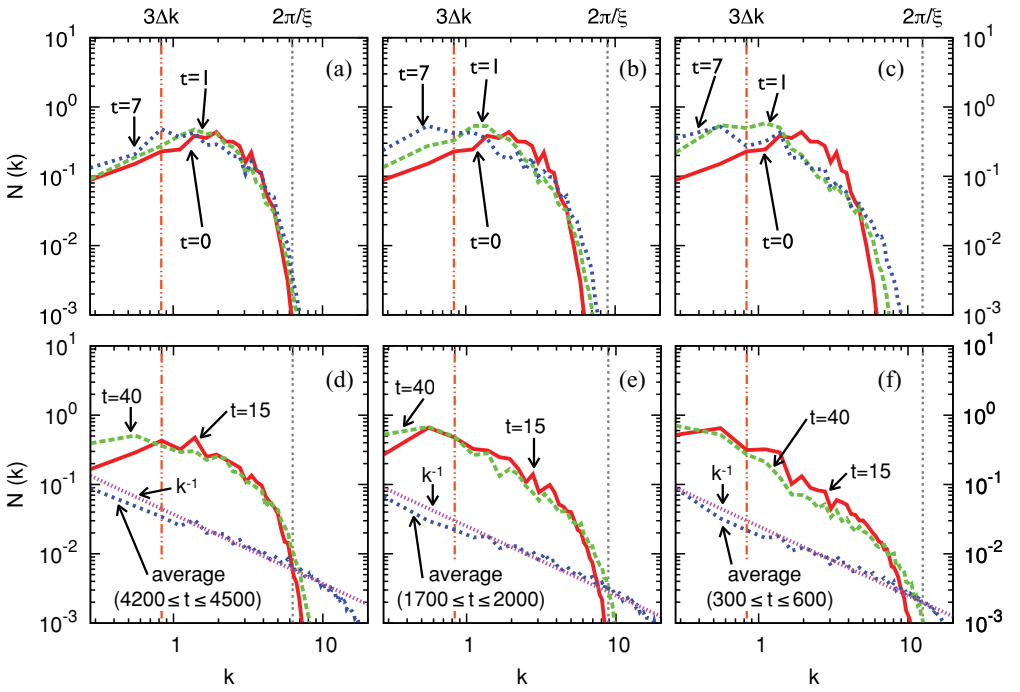

FIG. 5. (Color online) Log-log plots of the particle number spectra at earlier (upper panels) and later (lower panels) moments of time. Left panels: $g = 1$. Middle panels: $g = 2$. Right panels: $g = 4$.

D. Incompressible kinetic energy flux

One of our aims is to estimate from numerics the value and direction of the energy flux over a variety of scales in the incompressible and compressible subsystems, $\varepsilon^{\rm i}(k,t)$ and $\varepsilon^{\rm c}(k,t)$. To do this we use the observation (see the lower panels Fig. 1) that during most of the evolution (say for $t > 2.5$) the total kinetic energy is practically conserved. We can then neglect the energy exchange between these subsystems. In contrast, there is a permanent energy flux from the incompressible to the compressible subsystem and this exchange has to be accounted for. Therefore the (approximate) balance equations for the energy densities $E^{\rm c}_{\rm kin}(k,t)$ and $E^{\rm i}_{\rm kin}(k,t)$, introduced by

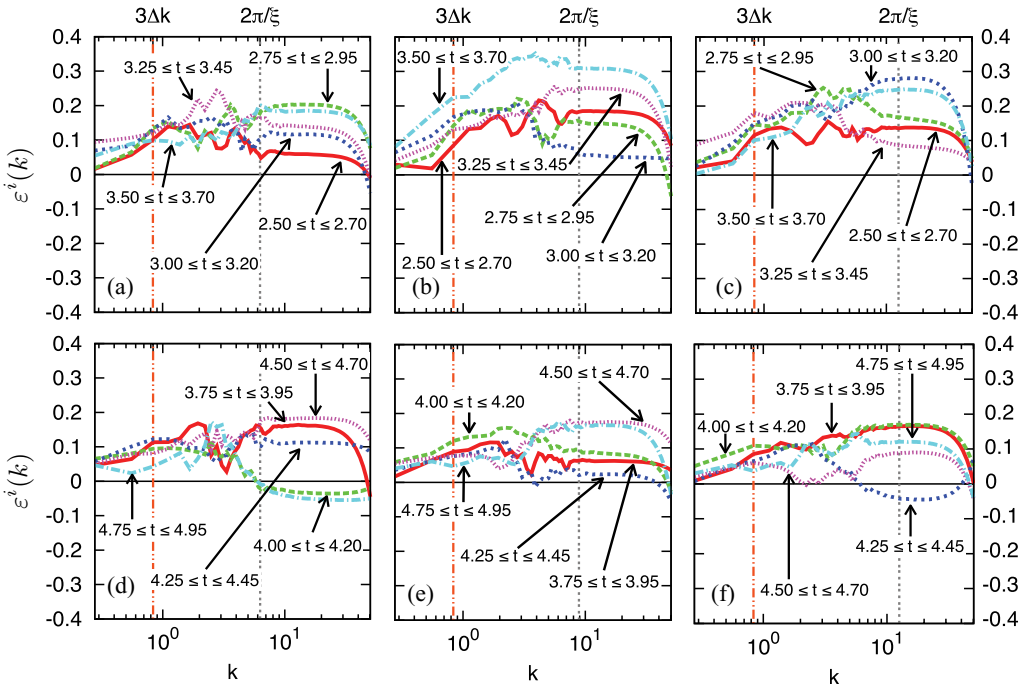

FIG. 6. (Color online) Averaged incompressible kinetic energy flux in a short time interval $\tau = 0.20$ in the time range $2.50 \leqslant t \leqslant 4.95$. Left panels: $g = 1$. Middle panels: $g = 2$. Right panels: $g = 4$.

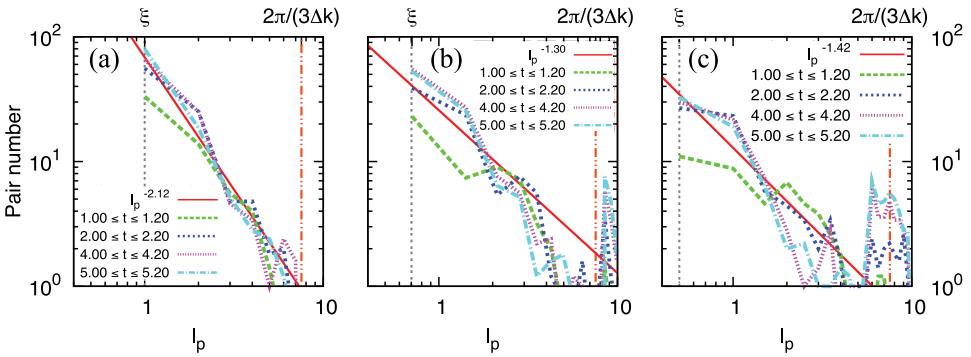

FIG. 7. (Color online) Averaged vortex pair number as the function of intervortex length l_p. Left panels: $g = 1$. Middle panels: $g = 2$. Right panels: $g = 4$.

Eqs. (11), can be written as follows:

$$\frac{\partial E^{\rm c}_{\rm kin}(k,t)}{\partial t} + \frac{\partial \varepsilon^{\rm c}(k,t)}{\partial k} + F^{\rm ci}(k,t) = 0, \tag{12a}$$

$$\frac{\partial E^{\rm i}_{\rm kin}(k,t)}{\partial t} + \frac{\partial \varepsilon^{\rm i}(k,t)}{\partial k} - F^{\rm ci}(k,t) = 0. \tag{12b}$$

Here $F^{\rm ci}(k,t)$ describes the energy exchange between subsystems. Integrating these equations we conclude

$$\varepsilon^{\rm c}(k,t) = -\int_{k_{\rm min}}^{k} \left[\frac{\partial E^{\rm c}_{\rm kin}(k',t)}{\partial t} + F^{\rm ci}(k',t)\right] dk', \tag{13a}$$

$$\varepsilon^{\rm i}(k,t) = -\int_{k_{\rm min}}^{k} \left[\frac{\partial E^{\rm i}_{\rm kin}(k',t)}{\partial t} - F^{\rm ci}(k',t)\right] dk'. \tag{13b}$$

A zero-order approximation is applied in the analysis of Eqs. (13) to eliminate $F^{\rm ci}(k,t)$ in these equations. This approximation can be improved as follows. We know that energy flux terms do not contribute to the total balance:

$$-\int_{k_{\rm min}}^{k_{\rm max}} \left[\frac{\partial E^{\rm c}_{\rm kin}(k',t)}{\partial t} + F^{\rm ci}(k',t)\right] dk' = 0, \tag{14a}$$

$$-\int_{k_{\rm min}}^{k_{\rm max}} \left[\frac{\partial E^{\rm i}_{\rm kin}(k',t)}{\partial t} - F^{\rm ci}(k',t)\right] dk' = 0, \tag{14b}$$

which allows us to find from numerics $\int_{k_{\rm min}}^{k_{\rm max}} F^{\rm ci}(k',t)dk'$ at any instant of time, for example, in the following way:

$$\int_{k_{\rm min}}^{k_{\rm max}} F^{\rm ci}(k',t)dk' = \int_{k_{\rm min}}^{k_{\rm max}} \frac{\partial\left[E^{\rm i}_{\rm kin}(k',t) - E^{\rm c}_{\rm kin}(k',t)\right]}{2\partial t} dk'. \tag{15a}$$

Next we can approximate $F^{\rm ci}(k',t)$ in the factorized form

$$F^{\rm ci}(k',t) \Rightarrow f(t)\varphi(k'), \tag{15b}$$

with a prescribed k'-dependent function $\varphi(k')$ that can be determined by reasonable physical arguments, for example, assuming that $F^{\rm ci}(k',t)$ mostly originates from the collapse of

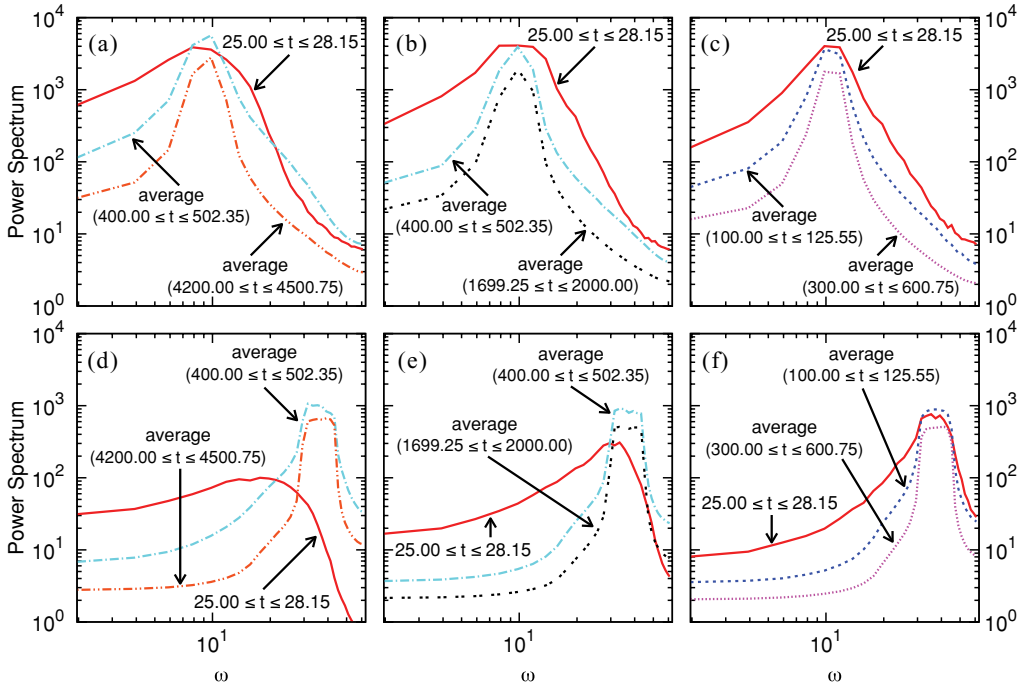

FIG. 8. (Color online) Log-log plots of the power spectra for the compressible velocity component with $k = 3\sqrt{2}$ (upper panels) and $k = 6\sqrt{2}$ (lower panels). Left panels: $g = 1$. Middle panels: $g = 2$. Right panels: $g = 4$.

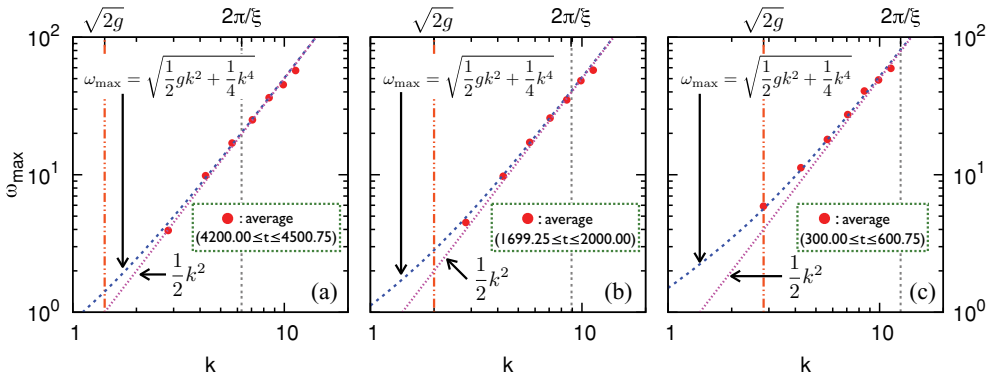

FIG. 9. (Color online) Position of the maximum frequency power spectra of the compressible velocity component for different wave vectors, averaged over a long time in the state of full thermodynamic equilibrium (full dots). Bogoliubov's frequency spectrum $\omega_{\max}(k)$, Eq. (21), and its large-k asymptotic $\omega_{\max}(k) \propto k^2$ are also shown. Left panel: $g = 1$. Middle panel: $g = 2$. Right panel: $g = 4$.

vortex pairs, and noting that the velocity around each vortex decays like $1/r'$, and giving in the k' representation an energy exchange proportional to k' and $E^{\mathrm{i}}_{\mathrm{kin}}(k') \propto k'|\tilde{\boldsymbol{w}}(k')|^2$. In our calculations we took $\varphi(k') \propto k'^3$, or in the normalized form

$$\varphi(k') = 4k'^3/k^4_{\max}. \tag{15c}$$

Then from Eq. (15a) we find

$$f(t) \approx \int_{k_{\min}}^{k_{\max}} \frac{\partial\left[E^{\mathrm{i}}_{\mathrm{kin}}(k',t) - E^{\mathrm{c}}_{\mathrm{kin}}(k',t)\right]}{2\partial t} dk'. \tag{15d}$$

Equations (15b), (15c), and (15d) can be substituted back into Eqs. (13) to get an improved approximation for the flux. Finally, we obtain the incompressible kinetic energy flux in a form with (15d):

$$\varepsilon^{\mathrm{i}}(k,t) \approx -\int_{k_{\min}}^{k} \frac{\partial E^{\mathrm{i}}_{\mathrm{kin}}(k',t)}{\partial t} dk' + f(t)\left(\frac{k}{k_{\max}}\right)^4. \tag{16}$$

Numerical results for the energy flux, obtained in this way, are shown in Fig. 6 and will be discussed later.

IV. DECAY OF 2D COMPRESSIBLE TURBULENCE

A. Free evolution of system energies and vortex number

Energy evolutions of the GP system, starting from the same initial condition $\Psi(\boldsymbol{r},0)$, but with different values of the coupling constant, $g = 1$, $g = 2$, and $g = 4$, are shown in

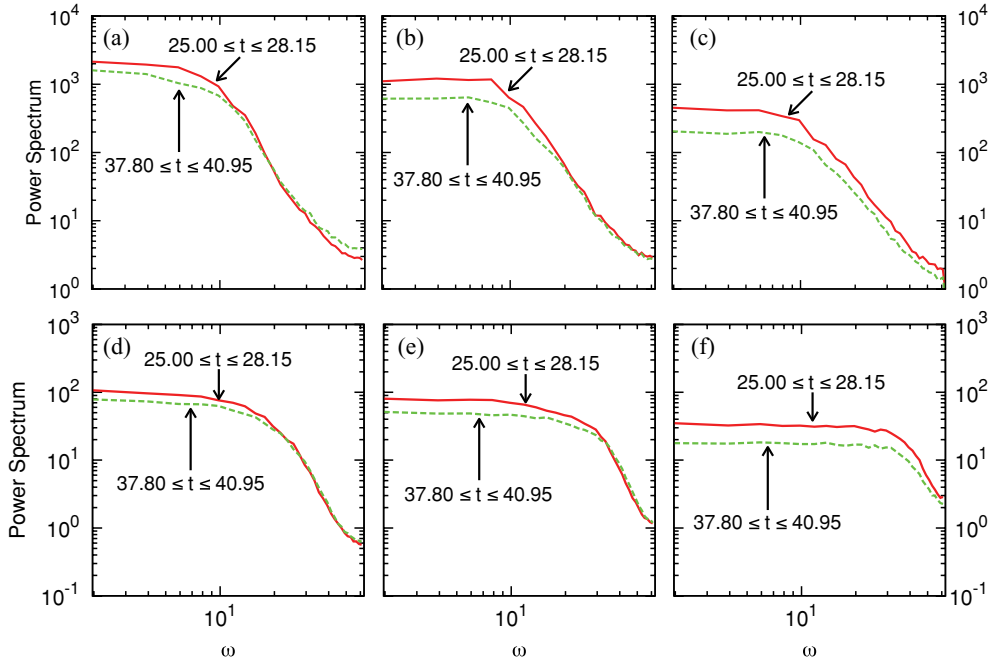

FIG. 10. (Color online) Log-log plots of the power spectra for the incompressible velocity component with $k = 3\sqrt{2}$ (upper panels) and $k = 6\sqrt{2}$ (lower panels). Left panels: $g = 1$. Middle panels: $g = 2$. Right panels: $g = 4$.

Fig. 1. Visual analysis of the figure leads to several qualitative statements concerning the system behavior:

(a) As expected, the total energy Hamiltonian is time independent and has larger values for larger g (due to the $g|\Psi|^4$ contribution).

(b) At the initial stages of the time evolution (for $t \lesssim 5$, upper panels) an intensive process of vortex creation leads to fast transformation of the compressible kinetic energy into incompressible kinetic energy and quantum energy (not shown). The incompressible kinetic energy is larger than the compressible kinetic energy for the time interval $2 \lesssim t \lesssim 4$.

(c) At later stages ($t \gtrsim 5$) the total kinetic energy is practically independent of time. Moreover its values are more or less the same for all g. This can be easily understood: The kinetic energy is quadratic in Ψ and does not contain the nonlinear term proportional to g.

(d) The largest maximal value of the vortex number $\mathcal{N}_{\rm qv}(t)$ is achieved at a smaller value $g = 1$ (left panel) at the crossover time $t \approx 5$. This is because for $t \gtrsim 5$ the probability of the dominant *nonlinear process* of vortex-pair annihilation is larger for larger g. We see that the fastest decay of $\mathcal{N}_{\rm qv}(t)$ corresponds to $g = 4$ (right panel).

(e) A faster decay of the vortex number for larger g leads to a larger increase in the flow compressibility with an increase in g. Correspondingly, the most compressible flow (largest value of the ratio $E^{\rm c}_{\rm kin}/E^{\rm i}_{\rm kin}$) is reached (in the presented data) for $g = 4$, and the least for $g = 1$.

(f) The system finally reaches its equilibrium state without quantized vortices for all g. It takes longer to reach its thermodynamic equilibrium state for smaller g.

(g) To clarify in more detail why a large value of the coupling g corresponds to a faster time evolution, we compute and plot in Fig. 2 the time evolution of the interaction energy $E_{\rm int}$, defined by Eq. (6) (and proportional to g). This energy has to be compared with the sum of the kinetic and quantum energies, $E_{\rm kin} + E_{\rm qnt}$, which originates from the quadratic term in the Hamiltonian (4a) or the linear term in the GPE (1). This sum is shown in Fig. 2. We see that typically $E_{\rm int}$ is essentially smaller than $E_{\rm kin} + E_{\rm qnt}$ and decays in time. Therefore the ratio

$$R \equiv E_{\rm int}/(E_{\rm kin} + E_{\rm qnt}), \tag{17}$$

shown in Fig. 2, characterizes how far our system deviates from its linear approximation. Accordingly, the ratio R can be called the *nonlinearity level*. The larger R is, the more quickly the system should evolve to its equilibrium state. Indeed, we see that the maximal value of $R \simeq 0.8$ is reached (at $t \approx 0.8$) for $g = 4$, while for $g = 1$ the maximal is $R \approx 0.2$, as expected. An important point is that R is essentially less than unity (e.g., $R \sim 0.2$ for $g = 4$ is the highest nonlinearity level at times $1.5 < t < 5$) and decreases with time. This means that in an analytical approach to the problem, the interaction can be treated through a perturbation approach with respect of R.

B. Evolution of the compressible and incompressible kinetic energy spectra

The energy distribution between scales (energy spectra) for $g = 1$, 2, and 4 and at different moments of time during free decay are shown in Fig. 3 for the compressible subsystem and in Fig. 4 for the incompressible subsystem. We conclude the following:

(a) At earlier stages (upper panels in both Figs. 3 and 4) the compressible and incompressible kinetic energies, being initially located at small $k \leqslant 3\Delta k$, propagate toward larger k, still (almost) monotonically decaying toward large k.

(b) The intermediate moments of time (around $t \sim 3$) will be discussed in detail in Sec. IV D. Here we only note that the incompressible spectra are close to the Kolmogorov-Obukhov law $E^{\rm i}_{\rm kin}(k) \propto k^{-5/3}$ shown in the upper panels of Fig. 4. This behavior is related to the energy cascade.

(c) At later times the energy begins to accumulate at large k and the energy spectra asymptotically approach the quasistationary state (practically coinciding, e.g., for $t = 15$ and $t = 40$ within the error bars, related to the lack of statistical averaging).

(d) The compressible energy spectra $E^{\rm c}_{\rm kin}(k)$ at this stage are close to the thermodynamic equilibrium with the energy equipartition between degrees of freedom. In 2D systems this gives (for one-dimensional spectra) $E^{\rm c}_{\rm kin}(k) \propto k$, as shown in the lower panels in Fig. 3. This state will be discussed in more detail in Sec. IV E.

(e) The achieved (quasistationary) distribution of the incompressible kinetic energy $E^{\rm i}_{\rm kin}$ (lower panels in Fig. 4) *does not* correspond to the thermodynamic equilibrium, as we can naively expect. This is related to the fact that at these times the system *does not achieve full equilibrium*. Indeed, the lower panels in Fig. 1 show that the incompressible kinetic energy continues to converge to the compressible energy. We interpret this stage as a kind of flux (not thermodynamic) equilibrium, when the spectrum $E^{\rm c}_{\rm kin}(k)$ is determined by the energy flux from the incompressible to the compressible subsystem. We think that at these times the energy exchange within these subsystems (which should lead to thermodynamic equilibrium) plays a subdominant role.

(f) After a long time evolution, all the kinetic energy finally comes to comprise the compressible component. This is the full thermodynamic state. We show the long-time-averaged compressible kinetic energy spectra $E^{\rm c}_{\rm kin}(k)$. As expected, this is proportional to k.

C. Evolution of the particle number spectra

As we can see from Eq. (4b), the total particle number is quadratic in $\Psi(\boldsymbol{r})$ and therefore can be presented in the $\boldsymbol{k}$ representation by Eq. (11c), shown in Fig. 5 for different time intervals and all values of $g = 1$, 2, and 4. As we see, initially, $N(k)$ is localized in small k. Through the turbulent state, the spectrum asymptotically approaches the form $N(k) \propto k^{-1}$ in the wave number range $k \lesssim 2\pi/\xi$. To rationalize this behavior, we note that in the full thermodynamic equilibrium this dependence should be related to $E^{\rm c}_{\rm kin}(k) \propto k$. Indeed, in this state, the nonlinearity level, Eq. (17), is small, meaning that the interaction energy can be neglected in comparison with the kinetic and quantum energy. In addition, the quantum energy, which cannot be considered negligible, corresponds to zero-point motion and this term does not give rise to particle currents [5]. Thus, only the kinetic energy spectrum is related to the particle spectrum. Moreover, almost all the kinetic

energy becomes the compressible component and there are no vortices, and as a result θ has no singularities and becomes of order unity. Thus the kinetic energy density can be estimated using a wave number k as follows:

$$\mathcal{E}_{\rm kin} \simeq \mathcal{E}^{\rm c}_{\rm kin} \simeq \tfrac{1}{2}\rho|\nabla\theta|^2 \sim \tfrac{1}{2}\rho k^2|\theta|^2 \sim \tfrac{1}{2}\rho k^2, \qquad (18)$$

which becomes in $\boldsymbol{k}$ space, using (11a) and (11c), $\frac{1}{2}|\tilde{\boldsymbol{w}}(\boldsymbol{k})|^2 \simeq \frac{1}{2}k^2|\tilde{\Psi}(\boldsymbol{k})|^2$, as a result,

$$E^{\rm c}_{\rm kin}(k) \simeq \tfrac{1}{2}k^2 N(k). \qquad (19)$$

In this way, the two relations $E^{\rm c}_{\rm kin}(k) \propto k$ and $N(k) \propto k^{-1}$ hold simultaneously. This relation is similar to the relation between enstrophy Ω and kinetic energy E in 2D classical fluids.

D. Observation of 2D direct energy cascade

Returning to the discussion of Figs. 1 and 3, we note the following:

(a) The incompressible energy spectra at these times can be interpreted as closed to the classical Kolmogorov-Obukhov distribution $E^{\rm i}_{\rm kin}(k) \propto k^{-5/3}$, shown in the upper panels of Fig. 4.

(b) Bearing in mind that during the system evolution the kinetic energy clearly propagates from small k [where it was initially located in $E^{\rm i}_{\rm kin}(k)$] toward large k we conclude that at some region of the system parameters we can observe a *2D-direct energy cascade*, which has previously been observed only in 3D hydrodynamic systems.

(c) Numerical analysis of the incompressible kinetic energy flux supports this explanation (b). Using Eq. (16), we calculate the incompressible kinetic energy flux. Averaged data for a short time interval $\tau = 0.20$ with five sets of data are shown in Fig. 6. The flux $\varepsilon^{\rm i}(k)$ takes positive values for $3\Delta k \lesssim k \lesssim 2\pi/\xi$ at least for $2.50 \leqslant t \leqslant 4.95$. This strongly supports the occurrence of a 2D direct energy cascade. Moreover, owing to the second term in Eq. (16), especially effective for high wave numbers, $\varepsilon^{\rm i}(k)$ tends to vanish at $k_{\rm max}$.

(d) The Kolmogorov energy spectrum $E^{\rm i}_{\rm kin}(k) \propto k^{-5/3}$ was previously observed in decaying 2D turbulence in the GPE [8]. However, this observation was interpreted in terms of the known 2D turbulence inverse energy cascade, predicted by Kraichnan [18]. We think that this interpretation is mistaken. In particular, if this interpretation is true, this spectrum has to be followed by a k^{-3} spectrum for a direct enstrophy cascade according to Kraichnan's scenario. However, the authors of Ref. [8] "observe a k^{-6} dependence in this range", instead of a k^{-3} dependence.

(e) When the Kolmogorov-Obukhov spectrum is formed, a two-dimensional Richardson cascade can be seen. We can identify the cores of the quantized vortices by finding the phase defects of the wave function. Then, we choose the shortest intervortex pair length l_p for all vortices. In Fig. 7, the averaged vortex pair number $\mathcal{N}_{\rm pair}(l_p)$ is shown and is proportional to l_p^{-n}, where n depends on g and $1.30 \leqslant n \leqslant 2.12$. This power law suggests a self-similar spatial structure. For two-dimensional vortices, one of the most effective lengths, corresponding to the length of three-dimensional vortex ring, is the intervortex length. We conclude that Fig. 7 implies the following: First, vortex pairs with distances comparable to $2\pi/(3\Delta k)$ are created. Second, the vortex pair distance progressively decreases. Finally, when the vortex pair distance becomes comparable to ξ, the pair is annihilated.

E. Frequency power spectra and types of motions

1. Compressible type of motion

Important information about types of motion can be extracted from the frequency power spectrum, which is the Fourier transform of the different-time pair correlation function of the motion amplitude. For example, if an amplitude $A(t)$ oscillates with a particular frequency ω_0, that is, $A(t) = A_0\exp(i\omega_0 t)$, then

$$J(\tau) \equiv \langle A(t+\tau)A^*(t)\rangle = A_0^2\exp(i\omega_0\tau),$$

giving

$$\widetilde{J}(\omega) = \int J(\tau)\exp(-i\omega\tau)d\tau \propto \delta(\omega-\omega_0).$$

In other words, pure periodic motion with frequency ω_0 has a frequency power spectrum with a very intensive peak of zero width at $\omega = \omega_0$. It is easy to check that decaying oscillations $A(t) = A_0\exp(-\gamma t + i\omega_0 t)$ have the power spectrum

$$\widetilde{J}(\omega) \propto \frac{\gamma}{(\omega-\omega_0)^2+\gamma^2}, \qquad (20)$$

that is, a peak at frequency ω_0 and width γ, inversely proportional to the lifetime of the motion.

We observed exactly this kind of frequency power spectra for the compressible velocity component at later times, as shown in Fig. 8 for $k = 3\sqrt{2}$ and $k = 6\sqrt{2}$. As the system evolves to the thermodynamic equilibrium state, the power spectrum forms sharp peaks. This tendency is also seen in the frequency power spectrum of the wave function Ψ (not shown). We repeated this analysis for different k and in Fig. 9 we plot the position of the maxima of the frequency power spectra of compressible motion, averaged over a long time interval in the thermodynamic equilibrium state. Bearing in mind that for these periods the nonlinearity level R is very small (about 0.04 for $g = 4$ and even smaller for $g = 2$ and 1), one can consider these fluctuations as almost linear perturbations on the background of the rest state. The eigenfrequencies of these oscillations have been found by Bogoliubov [5] with the result

$$\omega_{\rm max} = \sqrt{\tfrac{1}{2}gk^2 + \tfrac{1}{4}k^4}, \qquad (21)$$

plotted in Fig. 9. The excellent agreement between the theoretical and numerical results indicates that the observed thermodynamical fluctuation of the compressible velocity component is indeed Bogoliubov's elementary excitations. The relatively small, but finite width of the observed peaks characterizes the finiteness of the lifetime of these fluctuations, caused by interaction of the fluctuations with different k-vectors.

2. Incompressible type of motion

What kind of frequency power spectrum can we expect for the incompressible type of motion? To answer this we note that an incompressible fluid exhibits vortex motions in which the lifetime and turnover time are of the same order. This

may mean that the position of the peak maximum ω_0 and its width γ must be of the same order of magnitude. Moreover, more detailed analysis shows that, due to symmetry, $\omega_0 \equiv 0$. In fully developed turbulence, the dimensional estimate of the Kolmogorov-Obukhov spectrum gives $\tau^{-1}(k) \simeq \varepsilon^{1/3}k^{2/3}$ for the inverse lifetime of vortices, where ε is the energy flux.

Under a trivial consideration we can expect $\gamma \simeq \tau^{-1}(k)$. However, this will be true only in the reference system comoving with the small vortices. In the laboratory reference system, where the mean velocity of the fluid is absent, we have to account for the sweeping of small vortices in the velocity field $\boldsymbol{V}$ of the largest vortices. This gives a Doppler shift of the peak position equal to $\boldsymbol{k} \cdot \boldsymbol{V}$. Noting that the turbulent velocity field is random, we average the shifted frequency peaks over the statistics of large-scale motions, in which positive and negative velocities have the same probability. As a result we do not shift the peak, but instead widen it to $\gamma(k) \simeq \sqrt{\langle V^2 \rangle}k$.

Qualitatively, this is what is seen in Fig. 10, where the frequency power spectrum of the incompressible effective velocity component with $k = 3\sqrt{2}$ and $k = 6\sqrt{2}$ are shown. As expected, they do not form sharp peaks. Also the peak widths for $k = 3\sqrt{2}$ (upper panels) are smaller than for $k = 6\sqrt{2}$ (lower panels). We consider these facts as additional support for the fact that incompressible motion demonstrates turbulent vortex behavior.

As we already demonstrated, $E^{\mathrm{i}}_{\mathrm{kin}}(t)$ approaches 0 after $t \lesssim 5$, taking a long time, and all the vortices finally entirely disappear. As a result, the compressible effective velocity component dominates in the thermodynamic equilibrium state.

V. CONCLUSION

In this paper we predict and numerically demonstrate a two-dimensional direct energy cascade with the Kolmogorov-Obukhov's $-5/3$ law in two-dimensional quantum turbulence with the two-dimensional Gross-Pitaevskii model. The cascade is mainly caused by the *compressibility* of Bose-Einstein condensates which forbids enstrophy conservation. A two-dimensional direct energy cascade has not previously been observed in typical two-dimensional classical turbulence in the decaying case, which features direct enstrophy cascade and self-organization of the system, because of the conservation laws of both energy and enstrophy.

In addition, we demonstrate that the turbulent state shifts to the thermodynamic equilibrium state full of elementary excitations without quantized vortices. The dispersion relation calculated from the frequency power spectrum of the compressible velocity components shows that the equilibrium state is filled with Bogoliubov excitations.

It is important to note that two-dimensional quantum turbulence is not restricted to theory. It is possible to design experiments of two-dimensional quantum turbulence in pseudo-two-dimensional atomic Bose-Einstein condensates, superfluid ^{4}He, and superfluid ^{3}He. For Bose-Einstein condensates, one can prepare the same initial condition as that of this simulation in several ways. One is to use the phase imprinting technique on Bose-Einstein condensates and the other is to use the inherent phase fluctuations which emerge at lower dimensions. The former may be the simplest way to create the initial state. In addition, in this simulation the size of the system of one direction L in x-y space is about 30 times as large as the healing length ξ. In Sec. II, the vertical extent of the cloud is $a_{\mathrm{hz}} = \sqrt{\hbar/2m\omega_{\mathrm{z}}} = a_{\mathrm{h}}/\sqrt{\lambda} = 1.90\ \mu$m. Thus, the particle number density $\rho \sim 10^3/(\pi a_{\mathrm{h}}^2 a_{\mathrm{hz}}) = 4.64 \times 10^{18}\ \mathrm{m}^{-3}$. Then, the healing length becomes $\xi = \hbar/\sqrt{2mg\rho} = 1.22\ \mu$m. As a result, the size of the system in x-y space must be $L \sim 2a_{\mathrm{h}} \sim 10\xi$ to see the effects discussed in this paper. In this way, one can prepare the initial condition of Bose-Einstein condensates.

So far, almost all studies of quantum turbulence have concentrated on the three-dimensional case, except for a few works [8,25]. However, at least in atomic Bose-Einstein condensates, the compressibility causes a significant change from two-dimensional classical turbulence, and in a certain parameter range two-dimensional quantum turbulence differs from two-dimensional classical turbulence. Thus, we are certain that the two-dimensional direct energy cascade in two-dimensional quantum turbulence provides an interesting phase of study of quantum turbulence.

ACKNOWLEDGMENTS

MT acknowledges the support of a Grant-in Aid for Scientific Research from JSPS (Grant No. 21340104) and a Grant-in Aid for Scientific Research on Priority Areas from MEXT (Grant No. 17071008). VL acknowledges the kind hospitality of Osaka City University and the support of the Japan Society for the Promotion of Science (Grant No. S-09147), where this project was started, and partial support of the European Community—Research Infrastructures under the FP7 Capacities Specific Programme, MICROKELVIN (Project No. 228464) and the US–Israel Binational Science Foundation (Grant No. 2008110).

[1] M. Anderson, J. Ensher, M. Matthews, C. Wieman, and E. Cornell, Science **269**, 198 (1995).
[2] K. B. Davis, M. O. Mewes, M. R. Andrews, N. J. van Druten, D. S. Durfee, D. M. Kurn, and W. Ketterle, Phys. Rev. Lett. **75**, 3969 (1995).
[3] C. C. Bradley, C. A. Sackett, J. J. Tollett, and R. G. Hulet, Phys. Rev. Lett. **75**, 1687 (1995).
[4] L. Pitaevskii and S. Stringari, *Bose-Einstein Condensation* (Oxford University Press, Oxford, 2003).
[5] C. J. Pethick and H. Smith, *Bose-Einstein Condensation in Dilute Gases*, 2nd ed. (Cambridge University Press, Cambridge, 2008).
[6] *Progress in Low Temperature Physics*, edited by W. P. Halperin and M. Tsubota (Elsevier, Amsterdam, 2009), Vol. 16.
[7] M. Tsubota, J. Phys. Soc. Jpn. **77**, 111006 (2008).
[8] N. G. Parker and C. S. Adams, Phys. Rev. Lett. **95**, 145301 (2005).

[9] M. Kobayashi and M. Tsubota, Phys. Rev. Lett. **94**, 065302 (2005); J. Phys. Soc. Jpn. **74**, 3248 (2005).
[10] M. Kobayashi and M. Tsubota, Phys. Rev. Lett. **97**, 145301 (2006).
[11] V. B. Eltsov, A. I. Golov, R. de Graaf, R. Hänninen, M. Krusius, V. S. L'vov, and R. E. Solntsev, Phys. Rev. Lett. **99**, 265301 (2007).
[12] P. M. Walmsley, A. I. Golov, H. E. Hall, A. A. Levchenko, and W. F. Vinen, Phys. Rev. Lett. **99**, 265302 (2007).
[13] V. B. Eltsov, R. de Graaf, R. Hänninen, M. Krusius, R. E. Solntsev, V. S. L'vov, A. I. Golov, and P. M. Walmsley, in *Progress in Low Temperature Physics*, edited by W. P. Halperin and M. Tsubota (Elsevier, Amsterdam, 2009), Vol. 16, p. 46.
[14] C. Nore, M. Abid, and M. E. Brachet, Phys. Rev. Lett. **78**, 3896 (1997); Phys. Fluids **9**, 2644 (1997).
[15] M. Abid, C. Huepe, S. Metens, C. Nore, C. Pham, L. Tuckerman, and M. Brachet, Fluid Dyn. Res. **33**, 509 (2003).
[16] J. Maurer and P. Tabeling, Europhys. Lett. **43**, 29 (1998).
[17] T. Araki, M. Tsubota, and S. K. Nemirovskii, Phys. Rev. Lett. **89**, 145301 (2002).
[18] R. H. Kraichnan, Phys. Fluids **10**, 1417 (1967).
[19] P. Tabeling, Phys. Rep. **362**, 1 (2002).
[20] J. R. Herring and J. C. McWilliams, J. Fluid Mech. **153**, 229 (1985).
[21] G. Boffetta, A. Celani, and M. Vergassola, Phys. Rev. E **61**, R29 (2000).
[22] J.-P. Laval, B. Dubrulle, and S. V. Nazarenko, J. Comput. Phys. **196**, 184 (2004).
[23] R. Numasato and M. Tsubota, J. Low Temp. Phys. **158**, 415 (2010).
[24] K. Kasamatsu, M. Tsubota, and M. Ueda, Phys. Rev. A **67**, 033610 (2003).
[25] T.-L. Horng, C.-H. Hsueh, S.-W. Su, Y.-M. Kao, and S.-C. Gou, Phys. Rev. A **80**, 023618 (2009).